Materials Letters 93 (2013) 243–246

Contents lists available at SciVerse ScienceDirect

Materials Letters

journal homepage: www.elsevier.com/locate/matlet

Assembled hollow and core-shell SnO_2 microspheres as anode materials for Li-ion batteries

Ruiqing Liu [a], Ning Li [a,*], Guofeng Xia [a], Deyu Li [a], Chen Wang [a], Ning Xiao [a], Dong Tian [a], Gang Wu [b]

[a] School of Chemical Engineering & Technology, Harbin Institute of Technology, Harbin, 150001, Heilongjiang, PR China
[b] Materials Physics and Applications Division, Los Alamos National Laboratory, Los Alamos, NM 87545, USA

ARTICLE INFO

Article history:
Received 9 June 2012
Accepted 16 October 2012
Available online 26 October 2012

Keywords:
Nanoparticles
SnO_2 microspheres
Crystal structure
Composite structure
Lithium ion battery

ABSTRACT

SnO_2 microspheres with controllable morphology were prepared via a hydrothermal-annealing method. The SnO_2 morphology can be tuned by using AlOOH sol and γ-Al_2O_3 as additive. The hollow SnO_2 microspheres with incomplete core-shell structure prepared with small amount of γ-Al_2O_3 presented the best cycling performance in Li-ion battery, exhibiting a specific capacity of 374.2 mAh g^{-1} up to 100 cycles. The superior performance can be mainly attributed to the formation of more and smaller SnO_2 hollow microspheres and partial core-shell SnO_2 microspheres resulting from the γ-Al_2O_3 condensation nucleus. The unique hollow and core-shell composite structure of SnO_2 is capable of reducing the volume changes during Li insertion–extraction.

1. Introduction

Currently, SnO_2 has been investigated as one of the most promising anode materials in Li-ion batteries (LIBs) owing to its high theoretical specific capacity (780 mAh g^{-1}), compared to currently used graphite anode [1–4]. However, a severe volume change of SnO_2 electrode usually occurs during the charge–discharge process [5], which leads to pulverization of electrode and rapid capacity degradation. Therefore, its practical application in LIB anode has been significantly limited yet.

In order to mitigate the pulverization problem and extend the cycle stability of SnO_2 electrode, SnO_2 particles integrated with carbon materials as inactive buffer layer were widely explored, due to their soft intrinsic quality and good electronic conductivity [6–8]. Recently, SnO_2 materials with various morphology were synthesized, such as nanorod arrays [3], nanotubes [9], nanocrystalline [10,11], and hollow nanostructures [12–14]. These explorations, in particular, the hollow microspheres of SnO_2 [4,13,14] indicated that optimal morphology of SnO_2 material can enhance structural stability substantially through mitigating the volume change during Li insertion–extraction.

In this work, carbon-free SnO_2 microspheres were prepared via a new hydrothermal-annealing process, which the resulting morphology of microspheres can be easily adjusted with AlOOH sol and γ-Al_2O_3. The correlation between electrochemical properties and the morphology of SnO_2 microspheres was established to guide further materials design and synthesis.

2. Experimental section

In order to prepare AlOOH sol, SB powder (ultra-pure quasi boehmite type aluminum hydroxide) was dissolved in deionized water with a concentration of 10 wt%. The suspension was stirred at room temperature, and its pH was adjusted to 4 by adding HNO_3. Then SB powder was calcined at 500 °C for 1 h to prepare γ-Al_2O_3.

In a typical synthesis approach, $CO(NH_2)_2$ (1.922 g) and $Na_2SnO_3 \cdot 3H_2O$ (1.2802 g) were dissolved in 320 mL water and ethanol (EtOH/H_2O=0.6, V/V) mixed solution. In this process, extremely small amount additive (0.0851 g AlOOH sol or 0.0072 g γ-Al_2O_3) was added into the mixed solution. After stirring the solution for 5 min at room temperature, it was transferred into a 400 mL Teflon-lined stainless steel autoclave for a treatment at 180 °C for 24 h. After cooling down, the produced white precipitation was collected by centrifugation and thoroughly washed with deionized water and ethanol before drying at 90 °C overnight. Then, the white sample was calcined at 500 °C for 1 h to obtain the light yellow powder. For a comparison, the control sample without addition was prepared under identical conditions as description in [4]. In this work, the SnO_2 samples derived from non-additive, AlOOH sol and γ-Al_2O_3 were labeled as S1, S2 and S3, respectively.

The prepared SnO_2 microspheres were characterized with X-ray diffraction (XRD, Rigaku D/MAX-RB), field-emission scanning

* Corresponding author. Tel.: +86 451 86413721.
E-mail address: lininghit@263.net (N. Li).

0167-577X/$ - see front matter © 2012 Published by Elsevier B.V.
http://dx.doi.org/10.1016/j.matlet.2012.10.072

electron microscopy (FESEM, Hitachi S4800) and high resolution transmission electron microscopy (HRTEM, FEI TECNAI G2).

Lithium sheets were used as counter electrode and reference electrode, and the working electrode consisted of 80 wt% SnO_2 microspheres, 10 wt% acetylene black and 10 wt% polyvinylidene fluoride (PVDF). 1 M $LiPF_6$ ethylenecarbonate (EC) and dimethyl carbonate (DMC) with volume ratio of 1:1 solution was used as electrolyte. In an argon-filled glove box, lithium sheet and the working electrode were assembled into a button cell (CR2025) with ca. 2 mg active species (SnO_2). Electrochemical tests were carried out at room temperature. The SnO_2 microspheres anodes were underwent the galvanostatic charge–discharge cycling method and cyclic voltammogram tests using a battery testing system (CT-3008 W, NEWARE) and an electrochemical workstation CHI660B, respectively. The galvanostatic charge–discharge tests were conducted at the rate of 0.1C ($1C = 780\ mA\ g^{-1}$) in the voltage window of 0.04–2 V (vs. Li/Li^+). The CV curves were measured in a potential range of 0.02–2.9 V (vs. Li/Li^+) at a scan rate of $0.5\ mV\ s^{-1}$. The weight of SnO_2 was used to calculate the capacity.

3. Results and discussion

Fig. 1(i) shows XRD patterns of SnO_2 microspheres prepared with and without additive. All the diffraction peaks can be well indexed to a tetragonal rutile structure of SnO_2 (cassiterite, JCPDS no. 41-1445), indicating a good phase purity. The nearly identical XRD patterns indicate that the small amount additive has little influence on SnO_2 crystal structure.

The morphology of samples was examined by SEM and TEM. Fig. 1(a) and (g) are cited from Ref. [4] to have a better understanding. It can be seen that the diameters of the SnO_2 microspheres observed in Fig. 1(a), (b) and (c) are ca. 200 nm (S1), ca. 500 nm (S2) and ca. 100 nm (S3), respectively. In Fig. 1(a) and (c), a unique feature of hollow microspheres for S1 and S3 is identified by the partially broken shells as marked by arrows. In good agreement with the observation in SEM, the TEM images Fig. 1(d) and (f) presents a typical hollow feature that a light interior zone surrounding by an outside dark ring for S1 and S3. It clearly shows that the suggested shell has a thickness of approximately 25 nm. In Fig. 1(e), SnO_2 microspheres (S2) exhibit a solid core with irregular fragments outside the microspheres walls. According to Fig. 1(g) and (h), SnO_2 nanoparticles with an average size of 10 nm anchored onto the hollow sphere shell of S1 and S3 can been seen apparently. Moreover, the morphology of

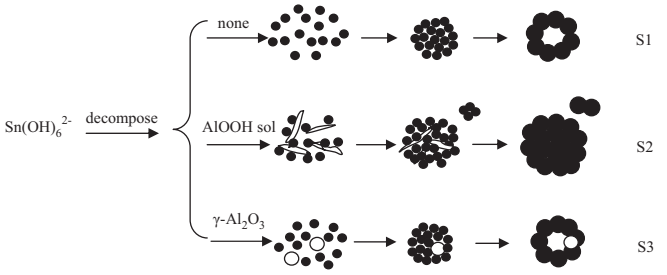

Scheme 1. The synthesis route of SnO_2 microspheres prepared with different additives.

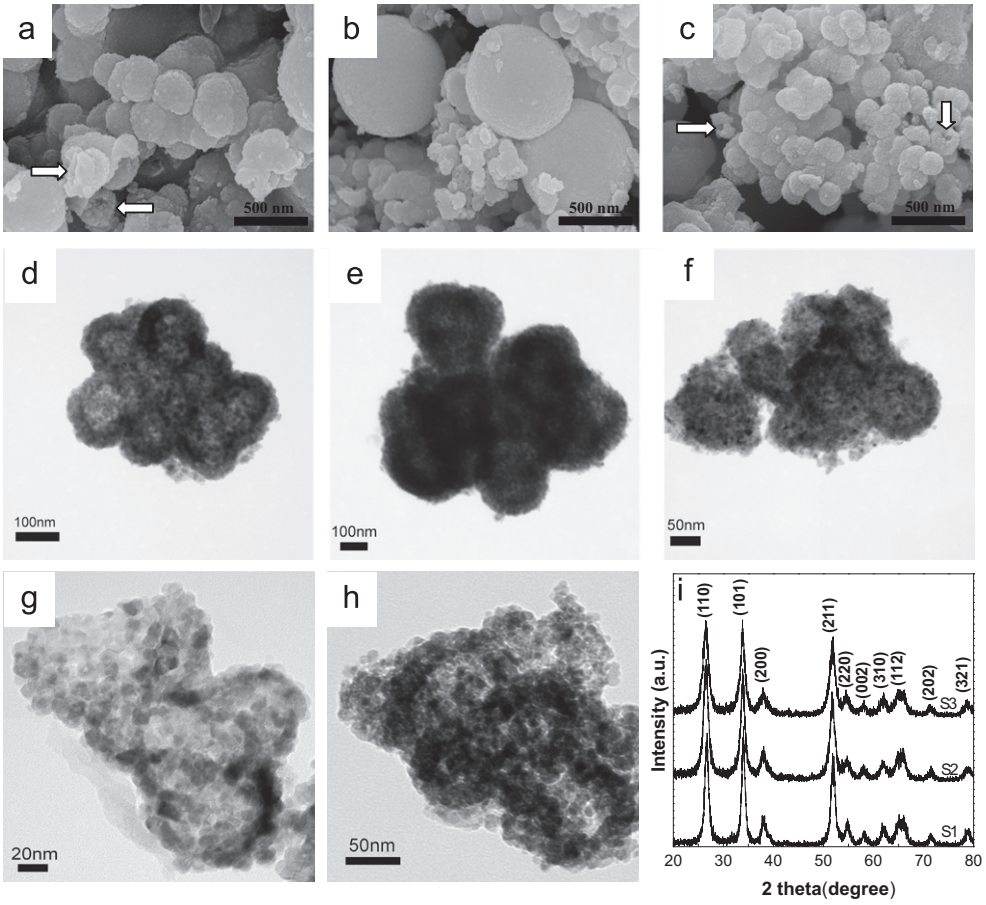

Fig. 1. SEM images in (a–c) and TEM images in (d–h) of different SnO_2 microspheres. S1 (a, d, g. a and g are cited from Ref. [4]), S2 (b, e) and S3 (c, f, h). XRD patterns in (i) of SnO_2 microspheres prepared with different additives.

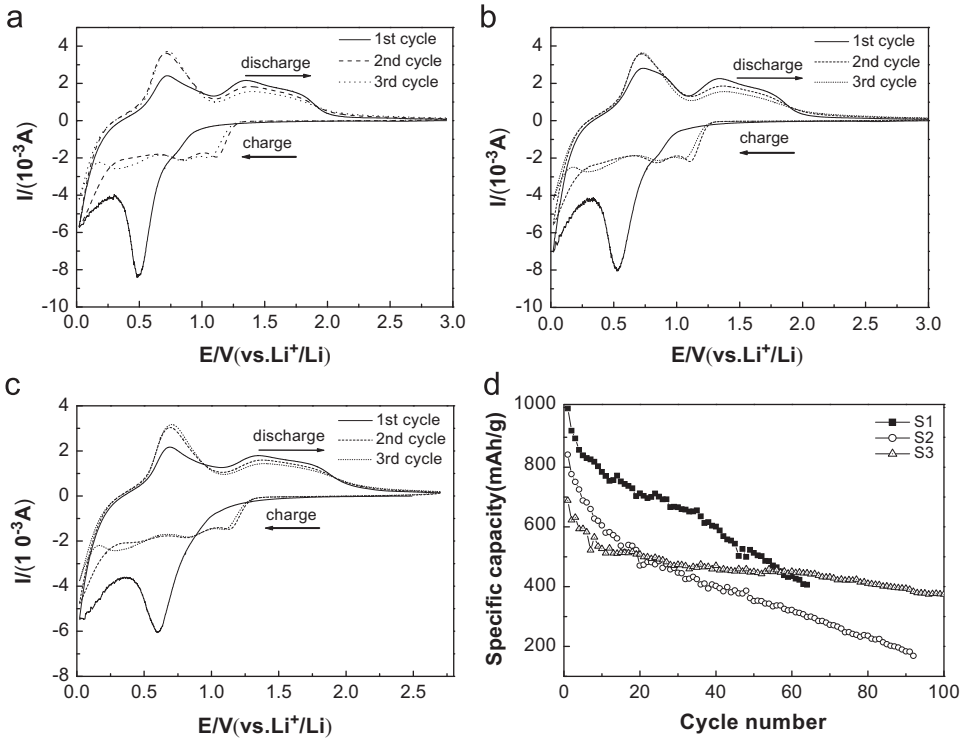

Fig. 2. The initial CV curves (a–c) and cycling discharge performance (d) for different SnO_2 microspheres anodes. S1 (a. from Ref. [4]), S2 (b) and S3 (c).

partial SnO_2 microspheres observed in Fig. 1(h) is a kind of core-shell assembly, which is named as hollow and core-shell composite structure.

It can be possible that SnO_2 hollow microspheres are grown through an "Ostwald ripening" mechanism [13]. As shown in Scheme 1 (S1), SnO_2 nanoparticles are formed by hydrolysis of stannate at the first stage, so as to minimize the overall energy of the system, then these nanoparticles tend to form the aggregated SnO_2 microspheres. Later, these solid microspheres are subject to inside-out ripening through consuming of inner active species and growing of surface sites on microspheres. However, AlOOH sol hinders the hollowing out process because of the influences from electric double layer of AlOOH sol colloidal particles, as well as the interaction between SnO_2 nanoparticles and AlOOH sol colloidal particles. In the meantime, the AlOOH sol hampers evacuation of inner nanoparticles, giving rise to a large internal stress of SnO_2 microspheres as shown in Scheme 1 (S2). On the other hand, when γ-Al_2O_3 powder dispersed in the SnO_2 nanoparticles, γ-Al_2O_3 acts as condensation nucleus (S3), facilitating formation of more and smaller SnO_2 microspheres during the first stage. The inside-out ripening process of microspheres is not affected by the presence of γ-Al_2O_3. As a result, incomplete core-shell structures are observed in the SnO_2 microspheres with a core of γ-Al_2O_3. The exact formation mechanism of SnO_2 microspheres prepared in this work is still unknown, and the effects of additive on self-assembly will be further determined.

The electrochemical measurements for different SnO_2 microspheres electrodes are shown in Fig. 2, and Fig. 2(a) is cited from Ref. [4] to have a better comparison. The CV curves of the three samples are similar. During the first cathodic scan, the peak at 0.5 V is ascribed to the reduction of SnO_2 to Sn and the formation of Li_2O as well as solid-electrolyte interface (SEI) [14]. The cathodic peak extending to 0.02 V and the anodic peak are assigned to the alloying and dealloying of Sn and Li, respectively [5]. Other peaks above 1.0 V seem possible due to the partially reversible reaction of Li_2O [14]. The three prepared SnO_2 microspheres exhibit different cycle performance. Fig. 2(d) indicated that retained specific capacity for each sample is 406.5 mAh g^{-1} up to 64 cycles for S1, 386.5 mAh g^{-1} up to 48 cycles for S2, and 374.2 mAh g^{-1} up to 100 cycles for S3. S3 exhibits the most excellent cycle performance as shown in Fig. 2(d), which is also higher than most SnO_2 nanostructures reported previously [4,10,15,16]. It's worth noting that the prepared SnO_2 hollow microspheres (S1) exhibit a better cycling performance than SnO_2 microspheres (S2). These results suggested that the hollow structured materials have advantages for the anode cycle performance [4,13,15]. The superior stability of S3 can be attributed to the formation of smaller SnO_2 hollow microspheres and incomplete core-shell structure. The interior microcavities of core-shell structured materials are capable of accommodating large volume change. In addition, the mutual support between core and shell heightens structural stability during Li insertion–extraction.

4. Conclusions

Morphology-controlled synthesis of SnO_2 microspheres was performed in this work by adding different additives, such as AlOOH sol and γ-Al_2O_3. The correlation between morphology and cycle performance indicated that the obtained hollow and incomplete core-shell composite structure in SnO_2 microspheres is a key to achieve high cycle performance as an anode material. The morphology assembly mechanism was discussed to explore the roles of AlOOH sol and γ-Al_2O_3 powder. In particular, as condensation nuclei, the γ-Al_2O_3 facilitates formation of more and smaller SnO_2 hollow microspheres with incomplete core-shell structure. The unique hollow and core-shell composite structure is found beneficial for alleviating the volume changes in lithium insertion–extraction. The current work may open a new way towards the development of SnO_2 anode materials in Li-ion batteries.

References

[1] Zhang YL, Liu Y, Liu ML. Chem Mater 2006;18:4643–6.
[2] Liu J, Xue DF. Electrochim Acta 2010;56:243–50.
[3] Lei DN, Zhang M, Hao QY, Chen LB, Li QH, Zhang ED, et al. Mater Lett 2011;65:1154–6.
[4] Liu RQ, Li N, Li DY, Xia GF, Zhu YM, Yu SY, et al. Mater Lett 2012;73:1–3.
[5] Courtney IA, Dahn JR. J Electrochem Soc 1997;144:2045–52.
[6] Wang Y, Lee JY. Electrochem Commun 2003;5:292–6.
[7] Derrien G, Hassoun J, Panero S, Scrosati B. Adv Mater 2007;19:2336–40.
[8] Hassoun J, Derrien G, Panero S, Scrosati B. Adv Mater 2008;20:3169–75.
[9] Li LM, Yin XM, Liu S, Wang YG, Chen LB, Wang TH. Electrochem Commun 2010;12:1383–6.
[10] Liang Y, Fan J, Xia XH, Jia ZJ. Mater Lett 2007;61:4370–3.
[11] Nuli YN, Zhao SL, Qin QZ. J Power Sour 2003;114(1):113–20.
[12] Yin XM, Li CC, Zhang M, Hao QY, Liu S, Chen LB, et al. J Phys Chem C 2010;114:8084–8.
[13] Lou XW, Wang Y, Yuan CL, Lee JY, Archer LA. Adv Mater 2006;18:2325–9.
[14] Liu HP, Long DH, Liu XJ, Qiao WM, Zhan L, Ling LC. Electrochim Acta 2009;54:5782–8.
[15] Han SJ, Jang B, Kim T, Oh SM, Hyeon T. Adv Funct Mater 2005;15:1845–50.
[16] Ye JF, Zhang HJ, Yang R, Li XG, Qi LM. Small 2010;6(2):296–306.